Stability Regions in the Parameter Space of PI Controller for LFC System with EVs Aggregator and Incommensurate Time Delays

Ausnain NAVEED
Department of Electrical and Electronics Engineering, Niğde Ömer Halisdemir University
Niğde, Turkey
husnain.naveed@gmail.com

Şahin SÖNMEZ
Department of Electrical and Electronics Engineering, Niğde Ömer Halisdemir University
Niğde, Turkey
sahinsonmez@ohu.edu.tr

Saffet AYASUN
Department of Electrical and Electronics Engineering, Niğde Ömer Halisdemir University
Niğde, Turkey
sayasun@ohu.edu.tr

***Abstract*— This paper presents a graphical method to compute all stabilizing Proportional Integral (PI) controller gains of a single-area Load Frequency Control (LFC) system with Electric Vehicles (EVs) Aggregator and multiple incommensurate communication time delays. The proposed approach is based on extracting stability region and the stability boundary locus in the PI controller parameter space. For various values of communication time delays, stability regions are obtained and the accuracy of Complex Root Boundary (CRB) and Real Root Boundary (RRB) are verified by means of quasi-polynomial mapping-based root finder (QPmR) algorithm and time-domain simulations.**

Keywords*— *communication time delays, electric vehicles, PI controller, load frequency control, stability region

I. INTRODUCTION

This work computes all stabilizing Proportional-Integral (PI) controller gains constituting a stability region in the controller parameter space of a single-area Load Frequency Control (LFC) system with Electric Vehicles (EVs) aggregator and multiple incommensurate communication time delays. Electric vehicles lie at the heart of modern power systems as rapid depletion of fossil resources and environmental changes are area of great concern. Batteries in EVs are capable of swiftly increasing and decreasing power output when compared with conventional generators. This swift response of EVs improves dynamic performance of LFC systems [1, 2]. For practical participation of EVs in frequency regulation market there should be a mechanism for aggregating and regulating large number of EVs and therefore, a new entity called EVs aggregator is used to satisfy the regulation criteria [3, 4]. For real-time scenarios, EVs must have a control system, automatic generation control (AGC) which can decide the power output increment or decrement of the batteries.

To communicate with this AGC, EVs require a dedicated or an open communication network. The latter is preferred due to low cost but it is prone to time delays in communication network. These delays can adversely affect LFC system dynamics and stability against an expectation that EVs can improve the LFC dynamic performance [5 ,6]. Hence, studying and investigating the time delays caused by the integration of EVs into the LFC system have a great significance. Many studies have been carried out to examine the effect of communication delays on the stable operation of conventional LFC systems without EVs. Mainly, that work aimed to determine the stability delay margin for which the system is marginally stable for given controller parameters. Time delay margin studies for LFC systems are mainly classified into two types of theoretical approaches. The first type is classified as indirect time-domain approach based on linear matrix inequalities and Lyapunov Stability Theory [7-10]. The second type is classified as frequency domain direct methods that aim to determine the critical eigenvalues or roots of the system and the corresponding stability delay margins [11, 12]. Both these approaches are capable of computing stability delay margins for any given PI controller parameters. Time-domain direct methods are applied to LFC system with EVs and time-varying communication delays [5, 6].

Both time-domain and frequency-domain methods can effectively compute delay margins for given controller gains. However, the main disadvantage of these methods is that one has to check the stability and compute the delay margin whenever the controller parameters are changed. This causes time-consuming checks for the stability computation. In order to sidestep this situation and thereby saving time for tuning the controller, it is essential to compute all possible controller gains that guarantee the stability of LFC system with EVs when a finite time delay is observed.

This paper presents a simple yet effective analytical approach to compute all stabilizing controller gains which constitute a stability region of LFC system with EVs in the parameter space of PI controller. The method relies on the computation of stability boundary locus by equating both the imaginary and real parts of the characteristic equation to zero [13,14]. The suggested method has been efficiently applied to single as well as two-area LFC system containing single delay without having EVs [15, 16], to the design of the conventional PI controller [17], fractional-order PD controller [18], and synthesis of PI controller for wind turbine systems [19].

In this paper, rather than a single communication delay, two incommensurate communication delays from PI controller to generator and to EVs aggregator are considered and stability regions are obtained for different delays. The exactness of region boundaries acquired by the suggested approach is authenticated by a quasi-polynomial mapping-based root finder (QPmR) algorithm. This algorithm is a numerical technique that determines the zeros of quasi-polynomials across large regions of the s-plane [20]. With the help of stability regions, one can easily adjust controller gains that will guarantee the stability of LFC systems with EV aggregator having time delays.

This work is supported by the Scientific and Technological Research Council of Turkey (TUBITAK) under Project No. 118E744.

978-1-5386-8086-5/19/$31.00 ©2019 IEEE

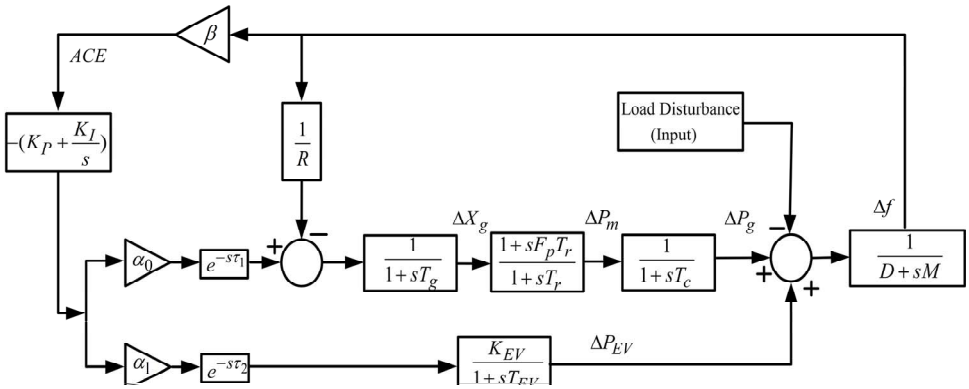

Fig. 1. Block diagram of a single-area LFC system with EVs aggregator.

II. Single-Area LFC with EVs Aggregator having Multiple Incommensurate Time Delays

The block diagram of a single-area LFC system including a single EV aggregator is given in Fig. 1. The dynamic model of the EV battery is described by the following first-order transfer function [5, 6]:

$$G_{EV}(s)=\frac{K_{EV}}{1+sT_{EV}} \tag{1}$$

where K_{EV} and T_{EV} represent the gain and the time constant of the EV battery system, respectively.

In Fig. 1, $\Delta f, \Delta X_g, \Delta P_m, \Delta P_g, \Delta P_{EV}$ and ΔP_d denote the deviation of frequency, valve position, mechanical power output, the generator power output, the EV aggregator power output and load disturbance, respectively. M, D, T_g, T_r, T_c, F_P , β and R are the generator inertia constant, damping coefficient, time constant of the governor, reheat-turbine, fraction of the total turbine power, frequency bias factor and speed drop, respectively. Moreover, ACE , K_P , and K_I represent the area control error, PI controller gains, respectively.

Because of any sudden changes in load demand, ACE as a control signal is transmitted to PI controller and then the output signal of the PI controller is send to reheat steam turbine and EVs aggregator based on the participation ratios α_0 and α_1 for the regulating of the system frequency. The control signals transmitted to EV aggregator through communication networks provide that EV participate in frequency regulation service to the grid. Note that the communication time delays from LFC controller to the conventional generator (τ_1) and from the EVs aggregator to the EV (τ_2) are considered to be incommensurate time delays [21] and these delay terms are modelled as exponential transfer function of $e^{-s\tau_1}$ and $e^{-s\tau_2}$ in Fig. 1.

The characteristic equation of the LFC system with the EVs aggregator is required to identify stability regions in PI controller parameter space. This equation is given as:

$$\Delta(s,\tau_1,\tau_2)=P(s)+Q(s)e^{-s\tau_1}+R(s)e^{-s\tau_2}=0 \tag{2}$$

where, τ_1 and τ_2 are the incommensurate time delays, $P(s)$, $Q(s)$ and $R(s)$ are the two polynomials in s having real coefficients in terms of system parameters. These polynomials and their coefficients are given as follows:

$$\begin{aligned} P(s)&=p_6s^6+p_5s^5+p_4s^4+p_3s^3+p_2s^2+p_1s\\ Q(s)&=q_3s^3+q_2s^2+q_1s+q_0\\ R(s)&=r_4s^4+r_3s^3+r_2s^2+r_1s+r_0 \end{aligned} \tag{3}$$

$$\begin{aligned} p_6 &= MRT_gT_rT_cT_{EV}\\ p_5 &= DRT_gT_rT_cT_{EV}+MRT_gT_rT_c+MRT_rT_cT_{EV}\\ &\quad +MRT_gT_cT_{EV}+MRT_gT_rT_{EV}\\ p_4 &= DRT_gT_rT_c+DRT_rT_cT_{EV}+DRT_gT_cT_{EV}\\ &\quad +DRT_gT_rT_{EV}+MRT_rT_c+MRT_gT_c+MRT_gT_r\\ &\quad +MRT_cT_{EV}+MRT_rT_{EV}+MRT_gT_{EV}\\ p_3 &= DRT_rT_c+DRT_gT_c+DRT_gT_r+DRT_cT_{EV}\\ &\quad +DRT_rT_{EV}+DRT_gT_{EV}+MRT_c+MRT_r\\ &\quad +MRT_g+MRT_{EV}+F_pT_rT_{EV}\\ p_2 &= DRT_c+DRT_r+DRT_g+DRT_{EV}\\ &\quad +MR+F_pT_r+T_{EV}\\ p_1 &= DR+1 \end{aligned} \tag{4}$$

$$\begin{aligned} q_3 &= \alpha_0\beta RK_pF_pT_rT_{EV}\\ q_2 &= \alpha_0\beta RK_pT_{EV}+\alpha_0\beta RK_pF_pT_r+\alpha_0\beta RK_IF_pT_rT_{EV}\\ q_1 &= \alpha_0\beta K_pR+\alpha_0\beta RK_IT_{EV}+\alpha_0\beta RK_IF_pT_r\\ q_0 &= \alpha_0\beta K_IR\\ r_4 &= \alpha_1\beta RK_{EV}K_pT_gT_rT_c\\ r_3 &= \alpha_1\beta RK_{EV}K_pT_rT_c+\alpha_1\beta RK_{EV}K_pT_gT_c\\ &\quad +\alpha_1\beta RK_{EV}K_pT_gT_r+\alpha_1\beta RK_{EV}K_IT_gT_rT_c\\ r_2 &= \alpha_1\beta RK_{EV}K_pT_c+\alpha_1\beta RK_{EV}K_pT_r\\ &\quad +\alpha_1\beta RK_{EV}K_pT_g+\alpha_1\beta RK_{EV}K_IT_rT_c\\ &\quad +\alpha_1\beta RK_{EV}K_IT_gT_c+\alpha_1\beta RK_{EV}K_IT_gT_r\\ r_1 &= \alpha_1\beta RK_{EV}K_p+\alpha_1\beta RK_{EV}K_IT_c\\ &\quad +\alpha_1\beta RK_{EV}K_IT_r+\alpha_1\beta RK_{EV}K_IT_g\\ r_0 &= \alpha_1\beta RK_{EV}K_I \end{aligned} \tag{5}$$

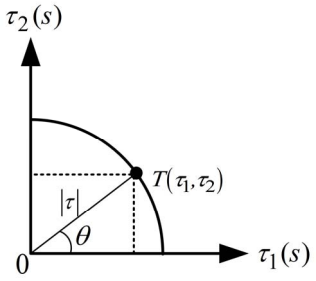

Fig. 2. Changing of τ_1 and τ_2 time delay values in a selected direction.

III. Computation of Stability Regions

A. Selection of Incommensurate Delays

The incommensurate time delays τ_1 and τ_2 are expressed in polar coordinate $(|\tau|,\theta)$ as shown in Fig. 2. All points are defined as $T(\tau_1,\tau_2)$ on a boundary depending on ($|\tau|$, θ) in (τ_1,τ_2)-space. Magnitude $|\tau|$ and angle θ are defined as $|\tau|=\sqrt{\tau_1^2+\tau_2^2}$ and $\theta=tan^{-1}\left(\frac{\tau_2}{\tau_1}\right)$. By changing the angle in a range of $\theta\in[0^0-90^0]$ while the magnitude $|\tau|$ is kept constant, the polar coordinate representation of these time delays will enable us to investigate the impact different delay cases such $\tau_1>\tau_2$, $\tau_1=\tau_2$ and $\tau_1<\tau_2$ on the stability regions.

B. Computation of Stability Regions in (K_P,K_I)-Plane

The identification of the stability region boundary for given time delays (τ_1,τ_2) or $(|\tau|,\theta)$ is achieved by substituting $s=j\omega_c$ when $\omega_c>0$ into the characteristic equation (2) given as follows:

$$\Delta(j\omega_c,\tau_1,\tau_2)=P(j\omega_c)+Q(j\omega_c)e^{-j\omega_c\tau_1}+R(j\omega_c)e^{-j\omega_c\tau_2}=0 \quad (6)$$

The main goal here is to compute the PI controller gains set (K_P,K_I) for which the characteristic equation of (6) will have purely imaginary roots on the $j\omega_c$-axis. The set of such (K_P,K_I) values defines the Complex Root Boundary (CRB) of the stability region. In order to determine this boundary, the coefficients of (6) can be re-written and controller gains are then separated to obtain a new equation as follows:

$$\begin{aligned}\Delta(j\omega_c,\tau_1,\tau_2)&=p_6(j\omega_c)^6+p_5(j\omega_c)^5+p_4(j\omega_c)^4\\&+p_3(j\omega_c)^3+p_2(j\omega_c)^2+p_1(j\omega_c)\\&+K_P[\{r_4'(j\omega_c)^4+r_3'(j\omega_c)^3+r_2'(j\omega_c)^2+r_1'(j\omega_c)\}e^{-j\omega_c\tau_2}\\&+\{q_3'(j\omega_c)^3+q_2'(j\omega_c)^2+q_1'(j\omega_c)\}e^{-j\omega_c\tau_1}]\\&+K_I[\{r_3''(j\omega_c)^3+r_2''(j\omega_c)^2+r_1''(j\omega_c)+r_0''\}e^{-j\omega_c\tau_2}\\&+\{q_2''(j\omega_c)^2+q_1''(j\omega_c)+q_0''\}e^{-j\omega_c\tau_1}]=0\end{aligned} \quad (7)$$

It is to be noted that q' and r' coefficients in (7) corresponds to the remaining terms in q and r in (5) after the terms that include K_P being extracted from them while q'' and r'' coefficients in (7) corresponds to the remaining terms in q and r in (5) after the terms that involve K_I being extracted from them.

By simplifying (7) further and setting both its real and imaginary parts of to zero, the following two equations are obtained;

$$\begin{aligned}K_PA_1(\omega_c)+K_IB_1(\omega_c)+C_1(\omega_c)=0\\K_PA_2(\omega_c)+K_IB_2(\omega_c)+C_2(\omega_c)=0\end{aligned} \quad (8)$$

The coefficients of $A_1(\omega_c),B_1(\omega_c),C_1(\omega_c),A_2(\omega_c),B_2(\omega_c)$ and $C_2(\omega_c)$ are given as:

$$\begin{aligned}A_1(\omega_c)&=r_4'\omega_c^4\cos(\omega_c\tau_2)-r_2'\omega_c^2\cos(\omega_c\tau_2)\\&-r_3'\omega_c^3\sin(\omega_c\tau_2)+r_1'\omega_c\sin(\omega_c\tau_2)\\&-q_2'\omega_c^2\cos(\omega_c\tau_1)-q_3'\omega_c^3\sin(\omega_c\tau_1)\\&+q_1'\omega_c\sin(\omega_c\tau_1)\\B_1(\omega_c)&=-r_2''\omega_c^2\cos(\omega_c\tau_2)+r_0''\cos(\omega_c\tau_2)-r_3''\omega_c^3\sin(\omega_c\tau_2)\\&+r_1''\omega_c\sin(\omega_c\tau_2)-q_2''\omega_c^2\sin(\omega_c\tau_1)+q_0''\cos(\omega_c\tau_1)\\&+q_1''\omega_c\sin(\omega_c\tau_1)\\C_1(\omega_c)&=-p_6\omega_c^6+p_4\omega_c^4+p_2\omega_c^2\\A_2(\omega_c)&=-r_3'\omega_c^3\cos(\omega_c\tau_2)+r_1'\omega_c\cos(\omega_c\tau_2)-r_4'\omega_c^4\sin(\omega_c\tau_2)\\&+r_2'\omega_c^2\sin(\omega_c\tau_2)-q_3'\omega_c^3\cos(\omega_c\tau_1)+q_1'\omega_c\cos(\omega_c\tau_1)\\&+q_2'\omega_c^2\sin(\omega_c\tau_1)\\B_2(\omega_c)&=-r_3''\omega_c^3\cos(\omega_c\tau_2)+r_1''\omega_c\cos(\omega_c\tau_2)+r_2''\omega_c^2\sin(\omega_c\tau_2)\\&+r_0''\sin(\omega_c\tau_2)+q_1''\omega_c\cos(\omega_c\tau_1)+q_2''\omega_c^2\sin(\omega_c\tau_1)\\&-q_0''\sin(\omega_c\tau_1)\\C_2(\omega_c)&=p_5\omega_c^5-p_3\omega_c^3+p_1\omega_c\end{aligned} \quad (9)$$

Two equations in (8) are simultaneously solved for (K_P,K_I) to identify the complex stability boundary locus $\ell(K_P,K_I,\omega_c)$ in the (K_P,K_I)-plane.

$$\begin{aligned}K_P&=\frac{B_1(\omega_c)C_2(\omega_c)-B_2(\omega_c)C_1(\omega_c)}{A_1(\omega_c)B_2(\omega_c)-A_2(\omega_c)B_1(\omega_c)}\\K_I&=\frac{A_2(\omega)C_1(\omega)-A_1(\omega)C_2(\omega)}{A_1(\omega_c)B_2(\omega_c)-A_2(\omega_c)B_1(\omega_c)}\end{aligned} \quad (10)$$

It should be observed from (8) and (9) that the line $K_I=0$ which is the K_P-axis in (K_P,K_I)-plane is also in the stability boundary locus because a real root of $\Delta(j\omega_c,\tau_1,\tau_2)=0$ in (7) could cross the imaginary axis at

$s = j\omega_c = 0$ only for $K_I = 0$. This boundary locus is called as the Real Root Boundary (RRB) of the stability region. Consequently, the CRB locus $\ell(K_P, K_I, \omega_c)$ and the RRB locus divide the (K_P, K_I) –plane into stable and unstable regions. The stable region gives a set of PI controller values for which (1) has all its roots in the left half of the s-plane indicating that the conventional LFC system with EVs aggregator is stable for the selected incommensurate time delays of (τ_1, τ_2).

IV. Results and Discussion

The section presents stability region results for the single-area LFC system with EVs aggregator and verification studies using the QPmR algorithm and time-domain simulations. The system parameters are given as follows [5]:

$$M = 8.8,\ D = 1,\ T_g = 0.2\ s,\ T_c = 0.3\ s,\ T_r = 12\ s,$$
$$F_P = 1/6,\ \mathrm{R} = 1/11,\ \beta = 21,\ K_{EV} = 1,\ T_{EV} = 0.1\ s$$

Recall that the selection of incommensurate delays (τ_1, τ_2) is achieved by using the polar coordinates and specifying the values of (τ_1, τ_2) by choosing $|\tau|$ and θ. In order to investigate the effect of different values of (τ_1, τ_2) on stability regions we first fix the angle at $\theta = 30^0$ and we obtain stability regions for four different $|\tau|$ values, $|\tau| = 0.5\ s, |\tau| = 0.8\ s, |\tau| = 1.0\ s, |\tau| = 1.2\ s$. The values of the corresponding incommensurate time delays (τ_1, τ_2) for this case is presented in Table I and stability regions are depicted in Fig. 3. This figure clearly illustrates that stability regions shrink as the magnitude of the delay increases from $|\tau| = 0.5\ s$ to $|\tau| = 1.2\ s$, resulting in smaller set of stabilizing PI controller gains for $\theta = 30^0$. Note that the angle $\theta = 30^0$ corresponds to the case in which the delay from LFC controller to the conventional generator is greater than the delay to the EVs aggregator to the EV, $\tau_1 > \tau_2$.

TABLE I. The Values Of (τ_1, τ_2) For $\theta = 30^0$

$\lvert\tau\rvert$	Incommensurate Time Delays (*s*)	
	τ_1	τ_2
0.5	0.433	0.25
0.8	0.693	0.4
1.0	0.866	0.5
1.2	1.045	0.6

Next, stability regions for $\theta = 45^0$ and 60^0 are obtained. The regions are presented in Fig. 4 and Fig. 5, respectively. The case of $\theta = 45^0$ corresponds to the case in which two delays are equal, $\tau_1 = \tau_2$. When the stability regions in Fig. 4 are compared with the ones in Fig. 3, it is clear that those regions are smaller than the ones for $\theta = 30^0$. This implies that a smaller set stabilizing PI controller parameters is obtained when $\tau_1 = \tau_2$ for all $|\tau|$. Fig. 5 illustrates stability regions for $\theta = 60^0$, which corresponds to the case of $\tau_1 < \tau_2$. Note that regions get even smaller which indicates that an increase in the delay on the EVs side τ_2 has a remarkable impacts on the size of regions.

Furthermore, the impact of angle θ on stability regions is investigated. Fig. 6 shows the stability regions for $\theta = 30^0, 45^0$ and 60^0 when magnitude of the delay is fixed at $|\tau| = 0.5\ s$. The size of stability regions decreases when θ angle is increased for $\theta \in \left[30^0 - 60^0\right]$. The outermost stability region for $\theta = 30^0$ implies that τ_1 is greater than τ_2 and thereby infers that the impact of delay due to conventional generator is more on the LFC system than the impact of delay due to EVs aggregator. The stability region in the center for $\theta = 45^0$ implies that τ_1 is equal to τ_2 and thereby infers that the impact of delay due to conventional generator is equal to the impact of delay due to EVs aggregator. Whereas the innermost stability region for $\theta = 60^0$ implies that τ_2 is greater than τ_1 and thereby infers that the impact of delay due to EVs aggregator is greater than the impact of delay due to conventional generator.

The stability regions give a set of PI controller gains such that the (2) has all its roots on the left half of the s-plane, which indicating the stable operation of the LFC system with EVs aggregator for those controller gains. This can be observed in Fig. 7(a) in which the time-domain simulation and the dominant roots distribution obtained using QPmR algorithm together with their zoom picture are illustrated for the point $(K_P = 3.9, K_I = 3.45)$ inside the stability region. This is the same region as shown in Fig. 3 for $|\tau| = 0.5\ s$ and $\theta = 30^0$. It is to be noted that the dominant roots are located in the left half the complex plane and oscillations in the frequency deviation are decaying, indicating the asymptotic stability. Fig. 7(b) illustrates that a complex conjugate roots pair will be located on the $j\omega$-axis for example $(K_P = 3.32, K_I = 3.45)$ chosen on the CRB locus and the LFC system with EVs aggregator will be marginally stable because of the sustained oscillations depicted in frequency response. As depicted in Fig. 7(c), the LFC system with EVs aggregator will become unstable due to a pair of complex roots located in the right half of the complex plane and the frequency response will have growing oscillations, for example $(K_P = 3.00, K_I = 3.45)$, selected outside the region.

The RRB locus is the K_P-axis $(K_I = 0)$ where the characteristic equation has a root at the origin and the remaining dominant roots are positioned in the left half s-plane, for example, $K_P = 3.00$, $K_I = 0.00$. This implies that the characteristic equation will have a positive real root and the system will become exponentially (non-oscillatory) unstable if PI controller gains are selected beyond the RRB or below the $K_P -$ axis. Fig. 8 clearly shows this case for $K_P = 3.00,$, $K_I = -0.25$.

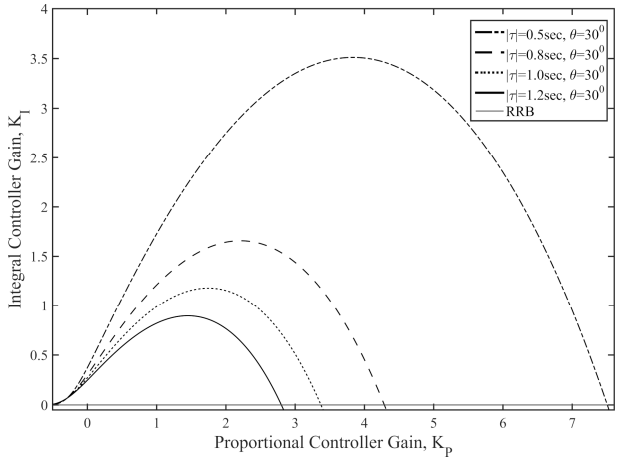

Fig. 3. Stability regions for different $|\tau|$ values at angle $\theta = 30^0$.

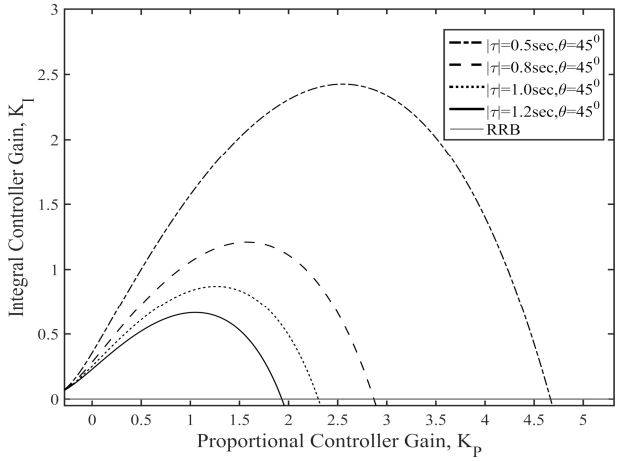

Fig. 4. Stability regions for different $|\tau|$ values at angle $\theta = 45^0$.

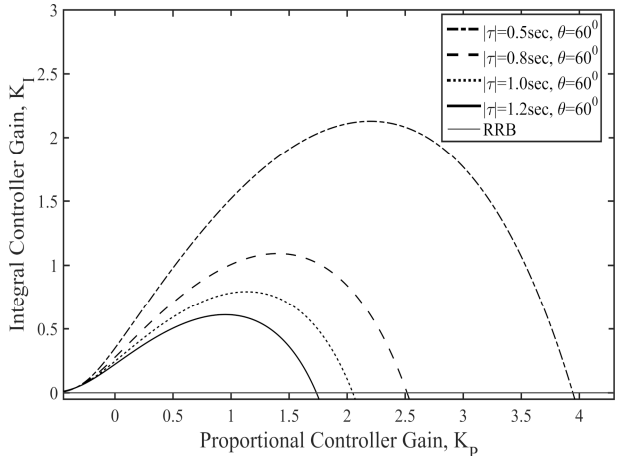

Fig. 5. Stability regions for different $|\tau|$ values at angle $\theta = 60^0$.

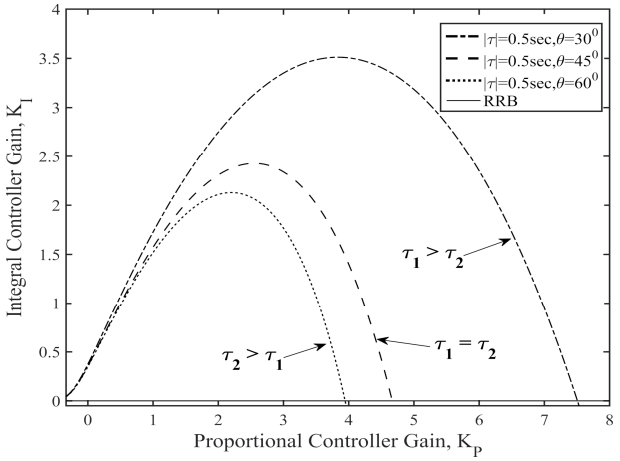

Fig. 6. Stability regions for the different values angle θ for $|\tau| = 0.5s$.

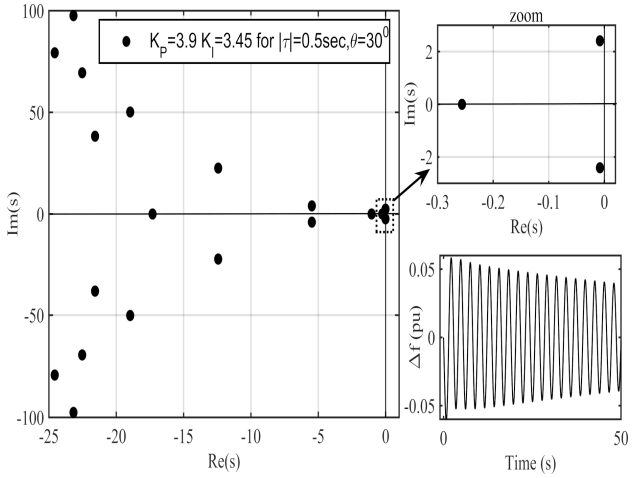

(a) Stable case

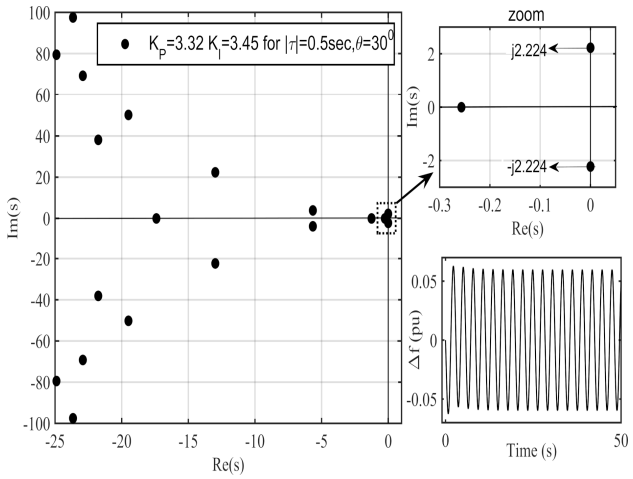

(b) Marginally stable case

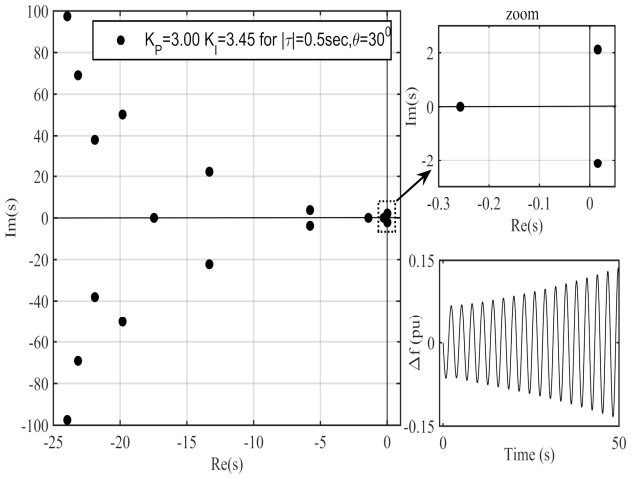

(c) Unstable case

Fig. 7. Dominant roots distribution of the characteristic equation around the CRB boundary and frequency response.

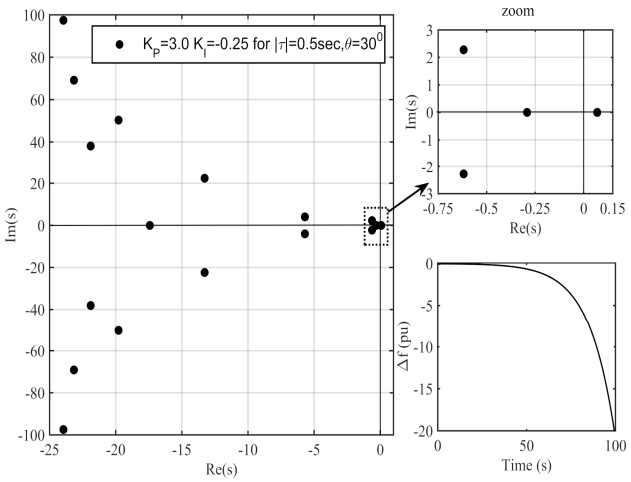

Fig. 8 Dominant roots distribution of the characteristic equation around the RRB boundary and frequency response.

V. CONCLUSIONS

This work presents a graphical approach that identifies the stability regions in the PI controller parameter space of a single-area LFC system with EVs aggregator having multiple incommensurate time delays. The stability regions provide all the stabilizing controller values that guarantee the stability of the LFC system with EVs aggregator having single-delayed conventional generator. Stability regions have been determined for different delay variation scenarios. It has been observed that the variation in the time delay on the EVs side significantly affects the size of stability regions.

Such stability regions enable appropriate selection of PI controller gains for which the LFC system with EVs aggregator having time delays will have a stable operation and thereby provide an ease in tuning those gains when variations are experienced.

REFERENCES

[1] W. Kempton and S. Letendre, "Electric Vehicles as a new power source for electric utilities," *Transportation Research* Part D. vol. 2, no. 3, pp.157-175. Sep. 1997.

[2] J. A Pecas Lopes, P. M. Rocha Almeida, and F. J. Soares, "Using vehicle to grid to maximize the integration of intermittent renewable energy resources in Islanded electric grids," in Proc. *Int. Conf. Clean Electr. Power Renew. Energy Res. Impact*, Capri, Italy, Jun. 2009, pp. 290–295.

[3] S. Han, S. Han, and K. Sezaki, "Development of an optimal vehicle-to-grid aggregator for frequency regulation," *IEEE Trans. Smart Grid*, vol. 1, pp. 65-72, June 2010.

[4] R. J. Bessa and M. A. Matos, "The role of an aggregator agent for EV in the electrical market," *Proc. 7th MedPower Conf.*, pp. 1-9, 2010.

[5] K. S. Ko and D. K. Sung, "The effect of EV aggregators with time-varying delays on the stability of a load frequency control system," *IEEE Trans. Power Syst*., vol. 33, no. 1, pp. 669 - 680, Jan. 2018.

[6] H. Jia, X. Li, Y. Mu, C. Xu, Y. Jiang, X. Yu, J. Wu, and C. Dong, "Coordinated control for EV aggregators and power plants in frequency regulation considering time-varying delay," *Applied Energy*, vol. 210, pp. 1363-1376, 2018.

[7] X. Yu and K. Tomsovic, "Application of linear matrix inequalities for load frequency control with communication delays," *IEEE Trans. Power Syst.*, vol. 19, no. 3, pp. 1508–1515, Aug. 2004.

[8] M. Liu, L. Yang, D. Gan, D. Wang, F. Gao, and Y. Chen, "The stability of AGC systems with commensurate delays," *Eur. Trans. Elect. Power*, vol. 17, no. 6, pp. 615–627, Nov./Dec. 2007.

[9] L. Jiang, W. Yao, Q. H. Wu, J. Y. Wen, and S. J. Cheng, "Delay-dependent stability for load frequency control with constant and time-varying delays," *IEEE Trans. Power Syst.*, vol. 27, no. 2, pp. 932–941, May 2012.

[10] C.-K. Zhang, L. Jiang, Q. H. Wu, Y. He, and M. Wu, "Further results on delay-dependent stability of multi-area load frequency control," *IEEE Trans. Power Syst.*, vol. 28, no. 4, pp. 4465–4474, Nov. 2013.

[11] N. Olgaç and R. Sipahi, "An exact method for the stability analysis of time-delayed linear time-invariant (LTI) systems," *IEEE Trans. Autom. Control,* vol. 47, no. 5, pp. 793-797, May 2002.

[12] Ş. Sönmez, S. Ayasun, and C. O. Nwankpa, "An exact method for computing delay margin for stability of load frequency control systems with constant communication delays," *IEEE Trans. Power Syst.*, vol. 31, no. 1, pp. 370-377, Jan. 2016.

[13] M. T. Söylemez, N. Munro, and H. Baki, "Fast calculation of stabilizing PID controller," *Automatica*, vol. 39, no. 1, pp. 121–126, 2003.

[14] N. Tan, I. Kaya, C. Yeroğlu, and D. P. Atherton, "Computation of stabilizing PI and PID controllers using the stability boundary locus," *Energy Convers. Manag*., vol. 47, no.18, pp 3045-3058, 2006.

[15] Ş. Sönmez and S. Ayasun, "Stability region in the parameter space of PI controller for a single-area load frequency control system with time delay," *IEEE Trans. Power Syst.,* vol. 31, no. 1, pp. 829–830, 2016.

[16] Ş. Sönmez and S. Ayasun, "Computation of PI controllers ensuring desired gain and phase margins for two-area load frequency control system with communication time delays," *Elect. Power Comp. Syst.*, vol. 46, no. 8, pp. 938-947, 2018.

[17] S. E. Hamamcı and N. Tan, "Design of PI controllers for achieving time and frequency domain specifications simultaneously," *ISA Trans.*, vol. 45, no. 4, pp. 529–543, 2006.

[18] S. E. Hamamcı and M. Köksal, "Calculation of all stabilizing fractional-order PD controllers for integrating time delays," *Comput. Math. Appl*., vol. 59, no. 5, pp. 1621–1629, 2010.

[19] J. Wang, N. Tse, and Z. Gao, "Synthesis on-PI-based pitch controller of large wind turbine generator," *Energy Convers. Manag.*, vol. 52, no. 2, pp. 1288–1294, 2011.

[20] T. Vyhlídal and P. Zítek "Mapping based algorithm for large-scale computation of quasi-polynomial zeros," *IEEE Trans. Autom. Control*, vol. 54, no. 1, pp 171-177, 2009.

[21] R. Krishnan, J. K. Pragatheeswaran, and G. Ray, "Robust stability of networked load frequency control systems with time-varying delays," *Elect. Power Comp. Syst.*, vol. 45, no. 3, pp. 302-314, 2017.